



## Thermally Reconfigurable Janus Droplets with Nematic Liquid Crystalline and Isotropic Perfluorocarbon Oil Compartments

Journal:	<i>Soft Matter</i>
Manuscript ID	SM-ART-12-2018-002600.R1
Article Type:	Paper
Date Submitted by the Author:	16-Feb-2019
Complete List of Authors:	Wang, Xin; Cornell University, Smith School of Chemical and Biomolecular Engineering Zhou, Ye; University of Chicago Division of the Physical Sciences, Kim, Youngki; Cornell University, Smith School of Chemical and Biomolecular Engineering Tsuei, Michael; Cornell University, Smith School of Chemical and Biomolecular Engineering Yang, Yu; University of Wisconsin-Madison, Chemical and Biological Engineering de Pablo, Juan J.; Liew Family Professor of Molecular Theory and Simulation, Institute for Molecular Engineering Abbott, Nicholas; Cornell University, Smith School of Chemical and Biomolecular Engineering

## Thermally Reconfigurable Janus Droplets with Nematic Liquid Crystalline and Isotropic Perfluorocarbon Oil Compartments

Xin Wang,<sup>‡a</sup> Ye Zhou,<sup>‡b</sup> Young-Ki Kim,<sup>a</sup> Michael Tsuei,<sup>a</sup> Yu Yang,<sup>d</sup> Juan J. de Pablo,<sup>\*b,c</sup> Nicholas L. Abbott<sup>\*a</sup>

Received 00th January 20xx,  
Accepted 00th January 20xx

DOI: 10.1039/x0xx00000x

www.rsc.org/

We report that mixtures of perfluorocarbon oils and hydrocarbon mesogens can be used to prepare multi-compartment (Janus) emulsion drops comprising coexisting nematic liquid crystalline (LC) and isotropic oil phases. The droplets exhibit stable spherical shapes with internal Janus-type morphologies that can be tuned widely through changes in temperature or adsorbates. In particular, we observe evidence of preferential adsorption of hydrocarbon or fluorocarbon surfactants on the interfaces of nematic versus isotropic domains, respectively, providing added control over the droplet structure. Comparisons of experiments and numerical simulations using a Landau-de Gennes continuum model provide insight into the relative importance of the LC elasticity and orientational-dependent interfacial energies on droplet morphologies and properties. We show that the hierarchical organization of the LC compartments generates optical properties and responsiveness not found in emulsions of isotropic oils.

### Introduction

Oil in water emulsions are encountered in a wide range of contexts<sup>1</sup>, including within foods<sup>2</sup>, in pharmaceutical preparations<sup>3</sup> and as templates for materials synthesis<sup>4,5</sup>. More recently, emulsion droplets with increasingly complex internal organizations have been explored, including multi-compartment droplets<sup>6–8</sup> and droplets comprised of structured oils such as liquid crystals<sup>9–12</sup>. The latter, in particular, offer the basis of systems that undergo changes in organization and optical properties in response to subtle stimuli such as bacterial lipids<sup>13,14</sup>, metabolites<sup>15</sup>, protein and cellulosic filaments<sup>16</sup>. In this paper, we report an investigation of multi-compartment emulsions where one compartment is a liquid crystalline (LC) oil and the other is an isotropic oil. The work is motivated by the long-range goal of designing complex emulsion droplets that possess morphological stability, yet can reorganize to generate optical responses to a range of triggers, including the presence of amphiphiles and targeted temperatures.

Multi-compartment emulsions comprised of coexisting isotropic oil domains have been widely investigated, and a thermodynamic framework has been established to describe droplet morphology<sup>7,17,18</sup>. In brief, the stability of Janus droplets (structured emulsions comprised of domains that

define two distinct faces) is determined by the interfacial tensions of the immiscible constituent phases (isotropic phases 1 and 2) and the third immiscible surrounding phase (phase 3; Fig. 1). Specifically, to form a Janus emulsion droplet, the three spreading coefficients  $S_i = \gamma_{jk} - (\gamma_{ij} + \gamma_{ik})$  ( $i \neq j \neq k = 1, 2, 3$ ) must all be negative. If this condition is not satisfied, either double emulsions with core-shell structures or separate droplets, each comprised of a single phase form at equilibrium. The morphology of a Janus droplet is described by the three interfacial tensions that form a Neumann's triangle, namely,

$$\frac{\gamma_{13}}{\sin \theta_2} = \frac{\gamma_{23}}{\sin \theta_1} = -\frac{\gamma_{12}}{\sin(\theta_1 + \theta_2)}.$$

This equation predicts that a Janus droplet comprised of two hemispheres ( $\theta_1 \rightarrow \pi/2$  and  $\theta_2 \rightarrow \pi/2$ ) will form if  $\gamma_{13} \sim \gamma_{23} \gg \gamma_{12}$ .

A range of experimental systems have been demonstrated to satisfy the above-described formalism, including systems comprised of isotropic phases of polymers, hydrocarbons and fluorocarbons<sup>7,18,19</sup>. In particular, the phase separation of isotropic hydrocarbon and fluorocarbon oils has been utilized to fabricate Janus droplets that, when combined with hydrocarbon and fluorocarbon surfactants, enabled access to

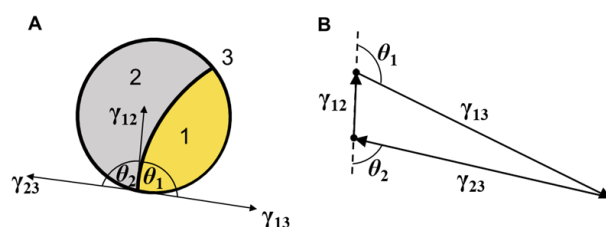


**Fig. 1** (A) Sketch of interfacial tensions of a Janus droplet that define (B) a Neumann's triangle and satisfy  $\gamma_{13} \sim \gamma_{23} \gg \gamma_{12}$ .

<sup>a</sup> Smith School of Chemical and Biomolecular Engineering, Cornell University, Ithaca, NY.

<sup>b</sup> Institute for Molecular Engineering, University of Chicago, Chicago, IL.

<sup>c</sup> Argonne National Laboratory, Chicago, IL.

<sup>d</sup> Department of Chemical and Biological Engineering, University of Wisconsin-Madison, WI.

<sup>‡</sup> Authors contributed equally.

† Electronic Supplementary Information (ESI) available. See DOI: 10.1039/x0xx00000x

various morphologies including Janus-type and core-shell structures<sup>20</sup>. The interfacial tensions between hydrocarbon and fluorocarbon compartments ( $\sim 1 \text{ mN m}^{-1}$ ) were an order of magnitude smaller than interfacial tensions at the oil-aqueous interfaces ( $\sim 10 \text{ mN m}^{-1}$ ), which endowed droplets with spherical shapes and mechanical stability in the presence of surfactants.

As noted above, single-compartment emulsion droplets comprised of liquid crystalline oils have also been reported<sup>4,10,21–34</sup>. These studies have revealed that the internal organization of the liquid crystal (LC) within the droplet reflects a delicate balance of contributions to the free energy that are absent in isotropic oil emulsions, including contributions arising from orientation-dependent interfacial free energies, elastic strain associated with deformation of the LC, and the presence of singular topological defects<sup>10,26,27</sup>. This balance of energetic contributions is strongly droplet-size dependent<sup>12</sup>, and can yield emulsion systems that reorganize in the presence of very low concentrations of amphiphilic species such as bacterial endotoxins<sup>13</sup>.

Whereas single-compartment LC droplets<sup>9,10,13–16,28</sup>, and multi-compartment isotropic emulsion droplets<sup>6–8,17–20</sup> have been explored, only a limited range of multi-compartment LC systems have been reported, the majority of which have been metastable liquid crystalline shells surrounded by inner and outer aqueous phases<sup>35–41</sup>. As described above, surface-energetic and elastic contributions to the free energy, as well as contributions to the free energy arising from formation of defects, depend strongly on geometry (topology), and thus we hypothesized that multi-compartment emulsions droplets with coexisting non-spherical LC and isotropic oil domains may offer access to both thermodynamic stability and responsiveness not found in spherically symmetric LC systems (shells). We note that one past study has reported Janus droplets formed of a liquid crystalline oil (5CB) and polymer (polydimethylsiloxane, PDMS) dispersed in aqueous solution<sup>42</sup>. The droplet morphology was demonstrated to be sensitive to surfactant concentration in the aqueous phase and the compartment volume ratio. The interfacial tensions of the three interfaces of the droplets, however, were similar in magnitude ( $\sim 1 \text{ mN m}^{-1}$ ), resulting in non-spherical droplets. In addition, in some instances, the Janus-type morphology was unstable (relative to two single-phase droplets) when surfactants were added.

In the experiments and simulations reported in this paper, we explore the morphologies and internal organization of Janus droplets with nematic and isotropic oil compartments formed using mixtures of hydrocarbon mesogens and isotropic fluorocarbon oils, namely, E7, a mixture of hydrogenated cyanobiphenyl and terphenyl mesogens that forms a nematic liquid crystalline phase at room temperature, and perfluorobenzene (FB), an isotropic fluorocarbon oil, respectively (Fig. 2). We used these two constituents to design thermally reconfigurable Janus droplets for three reasons. First, the temperature range over which nematic (N) and isotropic (I) phases coexist with typical thermotropic LCs is narrow (it is typically limited to 1–2 °C<sup>42–44</sup>). When using the mixture of E7 and FB, however, we found N-I coexistence to persist over an unusually broad temperature range ( $\sim 10 \text{ °C}$  at concentration of

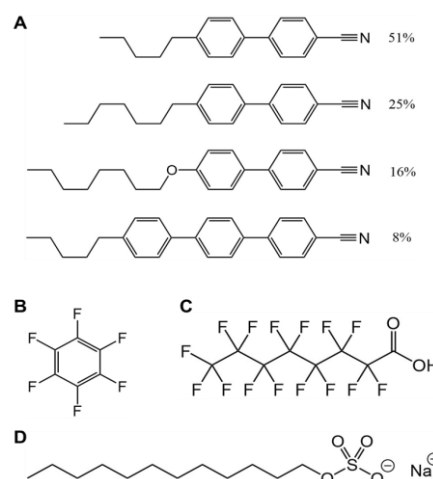


**Fig. 2** Molecular structures of (A) the mixture of nematogens called E7, (B) perfluorobenzene (FB), (C) perfluorooctanoic acid (PFOA) and (D) sodium dodecyl sulfate (SDS).

FB ( $C_{\text{FB}} = 10 \text{ % v/v}$ )<sup>45,46</sup>. This characteristic of the system enabled precise and continuous control over the morphologies of the droplets. As discussed below, the phase behaviour of this system also contrasts to previously studied two-phase isotropic perfluorocarbon/hydrocarbon systems<sup>6–8,27</sup>. Second, as both nematic and isotropic compartments are comprised of FB-E7 mixtures (the concentration difference between the two phases is less than 5 % v/v FB), the interfacial tension between the N-I compartments is small compared to the two oil-aqueous interfaces, and thus stable, spherical multicompartiment droplets were formed over a wide range of conditions (as internal structure varied). Third, whereas the similarity in composition of the two compartments is sufficiently small to provide stable droplets, the difference in composition between isotropic and nematic domains allowed control of the internal structures of the droplets by using either fluorocarbon or hydrocarbon surfactants. The choice of surfactant led to differential effects on the interfacial tensions of the hydrocarbon-rich (nematic) and perfluorocarbon-rich (isotropic) phases, resulting in surfactant-dependent changes in partial wetting of the internal phases on the aqueous interface of the droplets and thus morphology of the droplets. Additional insights regarding the interfacial energetics and internal ordering of the LC within the Janus emulsion droplets are described below by comparing experimental results and numerical simulations. Finally, we comment that an additional goal of our study was to determine if Janus droplets with nematic compartments deviate significantly from the above-described thermodynamic criteria used to describe the stability and morphology of Janus droplets comprised of isotropic oils.

## Experiments

### Materials

The nematic liquid crystal, E7, was purchased from HCCH (Jiangsu Hecheng Display Technology Co., LTD).

Hexafluorobenzene (99%, perfluorobenzene), toluene (anhydrous, 99.8%), n-hexane ( $\geq 99\%$ ), sodium dodecyl sulfate (99.0%, SDS) and perfluorooctanoic acid (96%, PFOA) were purchased from Sigma–Aldrich (St. Louis, MO, USA). Fisher Finest Premium Grade glass slides was purchased from Fisher Scientific (Pittsburgh, PA). Polyimide 2555, which was used to induce planar alignment of E7 when coated on glass substrates was purchased from HD Microsystems. Purification of water (18.2 M $\Omega$  cm resistivity at 25 °C) was performed using a Milli-Q water system (Millipore, Bedford, MA, USA).

### Preparation of Optical Cells

Optical cells were assembled from two glass slides separated from each other by either 20  $\mu\text{m}$ -diameter particles or 100  $\mu\text{m}$ -thick tape. Glass slides were spin-coated with polyimide 2555 using a Laurell spin coater, baked at 250 °C, and then rubbed and assembled in an anti-parallel fashion to yield unidirectional tangential alignment of LCs.

### Microscopy observations

Optical microscopy was performed using an Olympus BX41 microscope with a 20 $\times$  objective and a Moticam 10.0 MP camera. Temperature was controlled using a Linkam TMS 94 hot stage with an accuracy of 0.1 °C.

### Measurement of Phase Behavior of FB-E7 Mixtures

To measure the phase behavior of mixtures of E7 and FB, we prepared 5% v/v perfluorobenzene in E7 (FB-E7) by adding 20  $\mu\text{L}$  of perfluorobenzene to 400  $\mu\text{L}$  of nematic E7 at room temperature. Next, the mixture was vortexed at 3000 rpm for 10 seconds. The phase behavior of the FB-E7 mixture was measured using 20  $\mu\text{m}$ -thick optical cells and polarized light microscopy.

### Measurement of LC Orientation at Nematic-Isotropic (N-I) Interface

To characterize the orientation of the LC at the N-I interface, we prepared 5 % v/v FB-E7 mixture as described above, heated the mixture to an isotropic state at 55 °C (to avoid flow-induced alignment), and injected the mixture into a polyimide 2555-coated optical cell with a cavity thickness of 20  $\mu\text{m}$ . The sample was then cooled to 47 °C, at which temperature coexisting N and I phases were observed using optical microscopy.

### Preparation of Emulsions

To prepare droplets of FB-E7 stabilized by SDS, we dispersed 100  $\mu\text{L}$  of the 5 % v/v FB in E7 mixture described above in 1000  $\mu\text{L}$  FB-saturated aqueous SDS solution by vortexing at 3000 rpm for 8 seconds. The mixture was injected into a 100  $\mu\text{m}$ -thick optical cell at room temperature and sealed with silicone grease to prevent evaporation. The samples were equilibrated for 30 min prior to making observations.

To prepare droplets of FB-E7 stabilized by 1 mM of fluorocarbon surfactant (PFOA), we prepared 200 mM PFOA in FB, and then mixed 400  $\mu\text{L}$  E7 with 20  $\mu\text{L}$  of the PFOA dissolved

in perfluorobenzene. 100  $\mu\text{L}$  of the resulting FB-E7 mixture (containing 10 mM PFOA) was dispersed in 1000  $\mu\text{L}$  FB saturated 100  $\mu\text{M}$  SDS aqueous solution. This procedure resulted in an overall concentration of PFOA in the system of 1 mM. SDS was originally added to stabilize the droplets after vortex. We also dispersed PFOA-contained droplets in FB saturated water in the absence of SDS and non-PFOA droplets in the PFOA solution. We confirmed the internal structures of N-I biphasic droplets were similar.

### Measurement of Interfacial Tensions

We first prepared an 8 % v/v FB-E7 mixture by adding 32  $\mu\text{L}$  of perfluorobenzene to 400  $\mu\text{L}$  of E7 at room temperature. The resulting system was nematic at room temperature, and was heated to 36 °C to reach a biphasic state. The nematic and the isotropic phases were separated using an Eppendorf 5417R centrifuge for 15 min at 12000 rpm at 36 °C. The densities of the nematic and isotropic phases of the 8 % v/v FB-E7 mixture were 1.0462 g cm $^{-3}$  and 1.0487 g cm $^{-3}$ , respectively, measured with an Anton Paar DMA 5000 density meter. The interfacial tensions of the nematic-aqueous (N-A) interface,  $\gamma_{\text{N}}$ , the isotropic-aqueous (I-A) interface,  $\gamma_{\text{I}}$ , and the nematic-isotropic (N-I) interface,  $\gamma_{\text{N-I}}$  were measured using a Dataphysics OCA 15 plus contact angle measurement device with SCA 20 software. Pendant drops of LC were formed using Hamilton metal 22-gauge needles (blunt point). The equilibration time was 10 min for N-A and I-A interfaces, and 5 min for the N-I interface. Temperature was controlled using an environmental chamber with an accuracy of 0.1 °C. The 8 % v/v FB-E7 mixture was used in these experiments to ensure that coexistence of the N-I phases occurred within the operating temperature range of the centrifuge (−9 °C to + 40 °C). We confirmed that the 8 % v/v FB-E7 mixture did not have any qualitative difference compared to the 5 % v/v FB-E7 mixture in the experiments described in Fig. 5 and 8.

### Simulations

We used a Landau-de Gennes (LdG) continuum model for the order tensor  $\mathbf{Q}$ , defined by  $Q_{ij} = S(n_i n_j - 1/3 \delta_{ij})$ . Here,  $n_i$  are the  $x$ ,  $y$ ,  $z$  components of the local director vector $^{47}$ . The scalar order parameter is denoted by  $S$ . The bulk free energy is given by

$$F_{\text{bulk}}(\mathbf{Q}) = \int_{\text{bulk}} \left( \frac{A}{2} \left( 1 - \frac{U}{3} \right) Q_{ij} Q_{ji} - \frac{AU}{3} Q_{ij} Q_{jk} Q_{ki} + \frac{AU}{4} (Q_{ij} Q_{ji})^2 \right) dV + \int_{\text{bulk}} \frac{L}{2} \frac{\partial Q_{ij}}{\partial x_k} \frac{\partial Q_{ij}}{\partial x_k} dV$$

(1) where  $A$  and  $U$  are phenomenological parameters that depend on temperature and pressure. The one-constant representation is adopted here, where  $L$  denotes the elastic constant of the LC (the symbol  $K$  is used for the elastic constant in Frank-Oseen elastic energy and  $K = 2LS^2$ ).

The first term in Equation (1), which corresponds to enthalpic contributions to the free energy, serves to control the equilibrium value of the order parameter

$$S_{\text{eq}} = \frac{1}{4} \left( 1 + 3 \sqrt{1 - \frac{8}{3U}} \right)$$

The second term represents the elastic free energy, which governs long-range director distortions<sup>48</sup>.

The surface free energy, which represents the degenerate conic anchoring, was introduced in our previous work:

$$F_{\text{surf}}(\mathbf{Q}) = \int_{\text{surf}} W (P_{ik} \tilde{Q}_{kl} P_{lj} - S_{\text{cq}} \cos^2 \theta_e P_{ij})^2 d\Sigma \quad (2)$$

where  $W$  is the anchoring strength;  $\tilde{Q}_{ij} = Q_{ij} + (1/3) S_{\text{cq}} \delta_{ij}$ ; the preferred tilting angle between surface normal  $\nu$  and the 'easy cone' is denoted by  $\theta_e$ ; and the operator tensor  $P_{ij} = \nu_i \nu_j$ . The definition of operator tensor  $\mathbf{P}$  here is different from that in the Fournier-Galatola degenerate planar surface functional<sup>49</sup>. An iterative Ginzburg-Landau relaxation with finite difference method on a cubic mesh (with resolution of 7.15 nm) is adopted to minimize the free energy<sup>50</sup>. Polarization micrographs were calculated using the Jones matrix formalism, in which light of a single wavelength (350 nm) travels along a chosen direction and the total phase shift is accumulated<sup>51</sup>. The numerical parameters used in this work are  $A = 1.067 \times 10^5 \text{ J m}^{-3}$ ,  $U = 3.5$ ,  $L = 6 \text{ pN}$ , and  $K = 4.55 \text{ pN}$ . The droplet diameter  $D$  is  $2 \mu\text{m}$ <sup>52</sup>. The surface anchoring strengths are chosen according to experimental measurements.

## Results and discussion

### Phase behavior of E7-FB mixtures

To guide the design of Janus droplets using phase-separated mixtures of E7 and FB, we measured the temperature and composition-dependent phase behavior of FB-E7 mixtures. The inset in Fig. 3 shows that nematic domains dispersed in the isotropic continuous phase of a FB-E7 mixture (5 % v/v FB) at 44.0 °C were readily identified by optical microscopy as bright regions between crossed polars. Fig. 3 also shows that the phase diagram of FB-E7 mixtures comprises nematic (N), coexisting nematic-isotropic (N-I), and isotropic (I) regions. In the absence of FB, consistent with the Gibbs phase rule for a nematic mixture (Fig. 2), N and I phases coexist over a temperature range of  $\sim 2.4 \text{ }^\circ\text{C}$ <sup>53</sup>. Addition of FB to E7 decreases the N-I transition temperature ( $T_{\text{NI}}$ ) and leads to an expansion of the biphasic region. Specifically, for a mixture containing 10 % v/v FB, the temperature interval of the biphasic region expands to  $\sim 10 \text{ }^\circ\text{C}$ . We note that this temperature interval is wider than that for typical mixtures of hydrocarbons and E7. For example, the N-I coexistence of a mixture of E7 and hexane (10 % v/v) is  $\sim 4.8 \text{ }^\circ\text{C}$  (green triangles in Fig. 3), approximately one half that of the FB-E7 mixture. A toluene-E7 mixture (blue diamonds in Fig. 3) also possesses a N-I coexistence that is narrower than the FB-E7 mixture. The broad N-I coexistence of the FB-E7 mixture enables precise manipulation (via changes in temperature) of the relative volumes of the I and N compartments of Janus droplets. By separating nematic and

isotropic phases of an 8% v/v mixture of FB and E7 at 36°C, we found that the isotropic phase is FB-rich (12% v/v) relative to the coexisting nematic phase (7% v/v FB).

We hypothesized that the unusually broad biphasic region of the FB and E7 mixture occurred because of uneven partitioning of FB between the isotropic and nematic phases (i.e.,  $C_{\text{FB}}^{\text{I}}/C_{\text{FB}}^{\text{N}}$  is large). Past studies have reported that fluorine

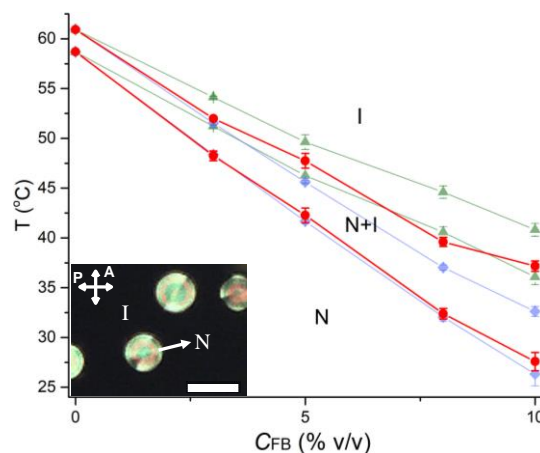


**Fig. 3** Phase diagram of the FB-E7 mixture (red circles ●), plotted as a function of volume fraction of FB ( $C_{\text{FB}}$ ). Mean  $\pm$  s.d. ( $n = 6$ ) are shown. The green triangles (▲) and the blue diamonds (◆) mark the limits of the N-I coexistence of hexane-E7 mixtures and toluene-E7 mixtures, respectively. The inset is an optical micrograph (crossed polars) of a FB-E7 mixture ( $C_{\text{FB}} = 5 \text{ } \%$  v/v) at 44.0 °C (N-I). Scale bar, 20  $\mu\text{m}$ . Double headed arrows indicate the orientation of polarizer (P) and analyzer (A).

atoms of the FB molecule withdraw electron density from the aromatic ring due to the high electronegativity of fluorine. Thus, the charge distribution of FB is opposite to that of benzene<sup>54</sup>. The resulting strong electrostatic attraction between FB and benzene has been shown previously (melting points at 5.0 °C and 5.4 °C, respectively) to lead to the formation of a solid complex containing equimolar quantities of the two compounds at 23.7 °C<sup>55</sup>. Within FB-E7 mixtures, we hypothesize that FB has a similar attraction to the aromatic rings of the biphenyls comprising E7, leading to a large ratio of activity coefficients for FB in nematic and isotropic phases, and thus a broad biphasic region (i.e.,  $C_{\text{FB}}^{\text{I}}/C_{\text{FB}}^{\text{N}}$  is large; see Supporting Information for additional discussion).

In the experiments reported below, we used mixtures of E7 and FB containing 5% v/v FB because it possesses a coexistence interval that starts 10 °C above room temperature (i.e., the mixture is homogenous at room temperature and the two-phase region can be conveniently accessed by heating from room temperature). We surveyed mixtures of FB and other thermotropic LCs, including 5CB (4-cyano-4'-pentylbiphenyl), 8CB (4'-n-octyl-4-cyano-biphenyl) and TL205 (a mixture of fluorinated biphenyl and terphenyl compounds that forms a nematic phase at room temperature). For each mixture containing 10% v/v FB, the temperature interval for N-I

coexistence was  $\sim 20$  °C below the N-I phase transition temperature ( $T_{NI}$ ) of the LC prior to addition of FB. Specifically, mixing FB with 5CB ( $T_{NI} = 35.5$  °C) or 8CB ( $T_{NI} = 40.5$  °C) results in a two-phase region below room temperature; while for TL205 ( $T_{NI} \sim 80$  °C), the temperature range of two-phase region is high ( $\sim 60$  °C). We also surveyed mixtures of perfluoroalkanes and these thermotropic LCs, but found them to be immiscible and to possess an upper consolute temperature similar to the isotropic systems reported in a past study<sup>20</sup>. The mixtures of perfluoroalkanes and LCs formed two-phase systems with coexisting phases that differed greatly in composition (close to 0% and 100%, perfluoroalkane, respectively) below the critical temperature, making it difficult to form stable, multicompartiment emulsions in the presence of the stimuli described in later parts of this paper.

#### Anchoring of nematic LC at interface to perfluorocarbon-rich isotropic phase

To understand the internal organization of multicompartiment emulsions based on FB and E7, a key underlying issue is the orientational ordering of the N phase at the interface of the I

phase (orientational anchoring). To provide insight into this issue, we performed experiments (Fig. 4) using films of the FB-E7 (5 % v/v) mixture confined between two polymer-coated glass surfaces that induced unidirectional tangential alignment ( $\mathbf{n}_o$ ) of LCs. The thickness of the LC film was 20  $\mu\text{m}$ . Fig. 4A and B show two N-I interfaces of a sample that have distinct orientations relative to the rubbing direction of the polymer film ( $\mathbf{n}_o$ ) at  $T = 47.0$  °C. When viewed between crossed polars, the interface (indicated by a blue frame) oriented parallel to the  $\mathbf{n}_o$  and polarizer (P) was bright (Fig. 4A), whereas the interface rotated from  $\mathbf{n}_o$  by  $40^\circ$  was dark (Fig. 4B). These observations are consistent with a tilted alignment ( $50^\circ$  with respect to the normal direction of N-I interface) of LC at the N-I interface. To exclude the possibility that the optical appearance in Fig. 4A was due to curvature of the N-I interface (i.e., a meniscus; the contact angle between the N-I interface and isotropic-glass interface was  $72^\circ$  (Fig. S1, ESI<sup>†</sup>)), we also examined a droplet of nematic LC dispersed in an isotropic continuous phase (Fig. 4C). The nematic domain was attached to one surface of the optical cell (did not span the thickness) and had a diameter less than 30  $\mu\text{m}$ . Inspection of Fig. 4C reveals a white band (indicated by a red frame) corresponding to a domain wall defect<sup>56</sup>, an

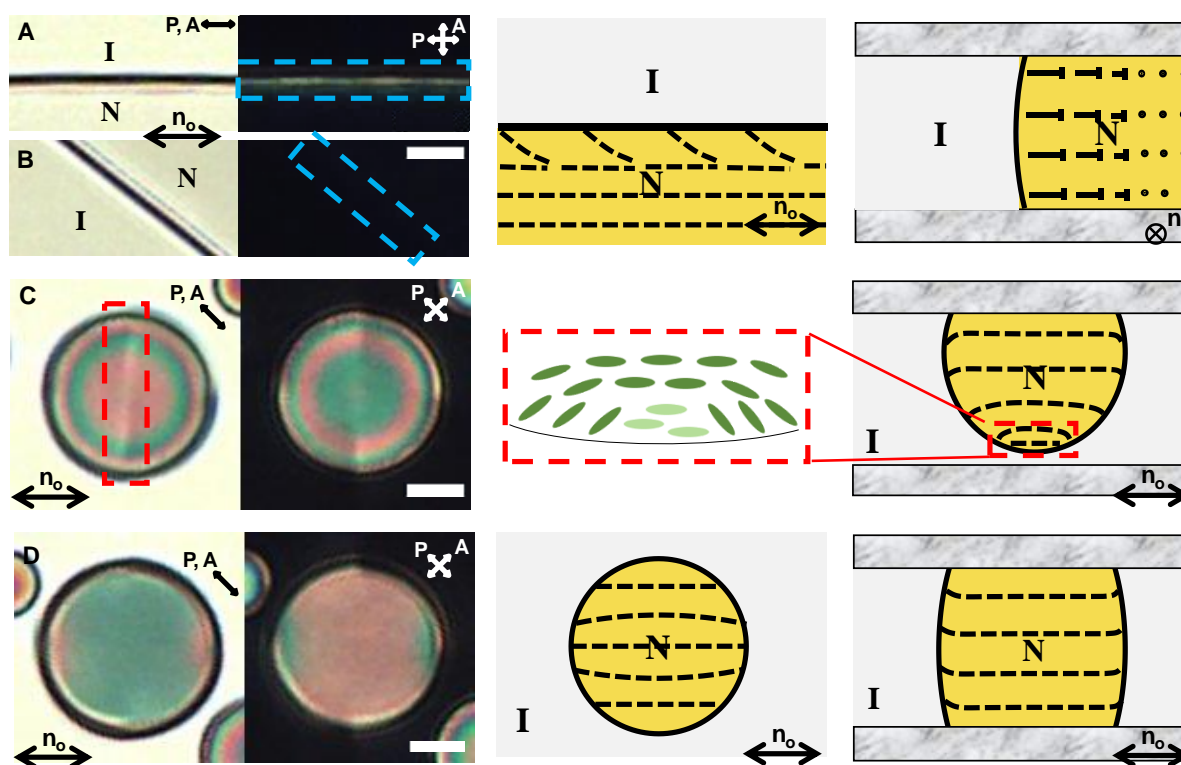


**Fig. 4** LC ordering at N-I interfaces of a FB-E7 mixture. (A) Optical micrograph (crossed polars) of N-I interface with an alignment that is parallel to the far field orientation of the LC ( $\mathbf{n}_o$ ) and (B) is inclined from  $\mathbf{n}_o$ . (Brightness and contrast of crossed-polarized micrographs in (A) and (B) are increased to enable visualization.) The schematic illustrations on the right side of A and B show an interface separating N and I domains as imaged in A, when viewed from the top (left illustration) or side (right illustration). (C) Optical image of a domain wall defect, indicated by the red frame, within a nematic domain attached to one surface of an optical cell. The schematic illustration to the right of C shows the LC orientations near the wall when viewed from the side. The green ellipsoids represent molecules in the nematic phase. (D) Optical image (crossed polars) of a cylindrical nematic domain spanning two surfaces. The schematic illustrations on the right are top and side views, respectively. Scale bars, 10  $\mu\text{m}$ . The anchoring of the LC at the confining surfaces is planar, and  $\mathbf{n}_o$  is parallel to the rubbing direction.

observation that is consistent with our conclusion of tilting of the LC at the N-I interface. Additionally, when the diameter of the nematic domain was larger than 30  $\mu\text{m}$ , the LC domain spanned the two glass surfaces and formed a cylindrical shape (Fig. 4D). The LC in the domain exhibited a uniform colour (green between parallel polars; red between crossed polars,) except at the two poles. The uniform colour indicates unidirectional alignment of the LC across the nematic domain, and thus weak surface anchoring of the LC at the N-I interface. The order of magnitude of the elastic modulus ( $K$ ) of E7 is  $\sim 5$  pN. To obtain an anchoring energy ( $\sim Wl^2$ ) that is comparable in magnitude to the elastic energy ( $\sim Kl$ ), we estimate the anchoring strength ( $W$ ) to be of order of  $10^{-6}$ - $10^{-7}$  N  $\text{m}^{-1}$ , where the length scale  $l$  is  $\sim 10$   $\mu\text{m}$ . This value is small compared to typical values of anchoring energies of LCs<sup>9,57</sup> (typically  $10^{-4}$ - $10^{-5}$  N  $\text{m}^{-1}$ ). Furthermore, the nematic domains we observed assumed a spherical shape (Fig. 4C and D), hinting that the elastic energy associated with confinement of the LC is small compared to the interfacial free energy. As detailed below, we use this experimental characterization of the N-I interface to provide boundary conditions for numerical simulations of the internal organization of the LC droplets.

#### Temperature-dependent morphology and internal ordering of complex LC emulsions

Next, we leveraged the above-described understanding of the phase behavior of the FB-E7 mixture and ordering at the N-I interface to prepare and provide insights into emulsions formed from E7 and FB mixtures. The FB-E7 mixture (5% v/v FB) was dispersed into aqueous SDS solution to explore the temperature-dependent droplet morphology and the ordering of LC within the nematic compartments. We prepared the dispersions by vortexing the mixture in the single-phase region of the phase diagram (room temperature) to ensure that the droplets were homogeneous in composition. As detailed below, we focus initially on the morphology of the emulsions; subsequently, we address internal ordering of LC domains.

Fig. 5 shows the morphologies of FB-E7 droplets observed as a function of increasing temperature in the presence of 1 mM SDS (the morphology and internal ordering is dependent on surfactant type and concentration; see Fig. 6 and 8). At 35  $^{\circ}\text{C}$ , the entire droplet volume was a single nematic phase (Fig. 5A). Optical images between crossed polars revealed a so-called radial configuration<sup>10</sup>, indicating a perpendicular alignment of the LC at the aqueous interface. The optical texture is characterized by a point defect at the center of droplets and Maltese cross between crossed polars. Upon heating the droplet above  $T_{\text{N-I}} = 42$   $^{\circ}\text{C}$ , we observed an isotropic domain to nucleate at the central defect (Fig. 5B and C). We hypothesized that nucleation of the isotropic phase occurred at the defect because of the high free energy density of the defect core<sup>9,58</sup>. The configuration shown in Fig. 5B was unstable and transient. The isotropic domain translated to the aqueous interface after formation. Fig. 5D shows a Janus morphology observed at  $T = 45.0$   $^{\circ}\text{C}$ . At 46.0  $^{\circ}\text{C}$ , the isotropic compartment expanded in volume, ultimately yielding a Janus droplet comprised of N and

I hemispheres of equal size (Fig. 5E). With further heating, the isotropic compartment expanded (Fig. 5F) to eventually occupy the entire volume of the droplet at 47.5  $^{\circ}\text{C}$  (Fig. 5G).

The sequence of morphological states of the droplet described above was largely reversible and seen to occur upon reducing the temperature (Fig. S3, ESI<sup>†</sup>). In brief, during the cooling process, we observed multiple nematic domains to nucleate at the aqueous interface and then to coalesce into a single nematic domain. This coalescence process is likely driven by minimization of both the elastic energy of the nematic LC and

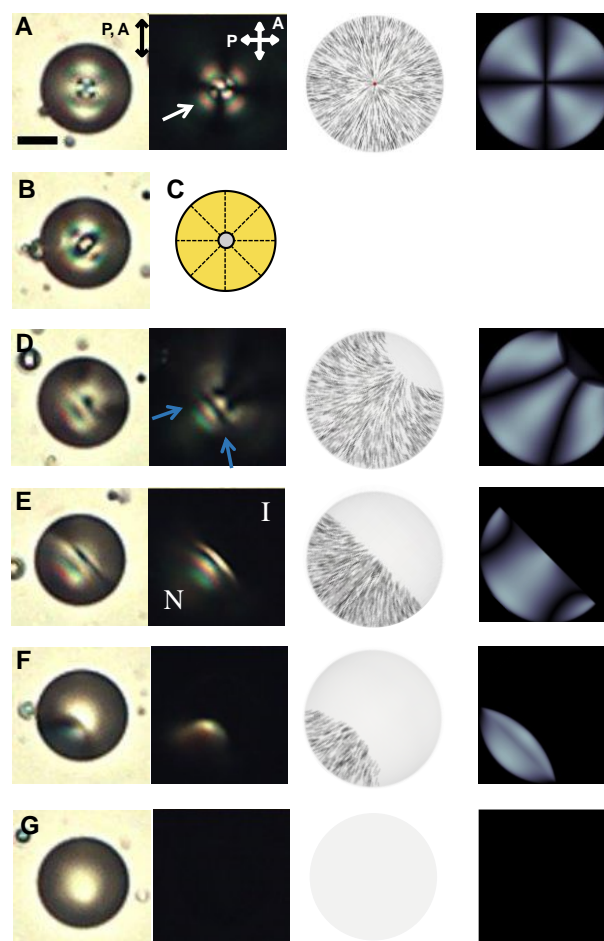


**Fig. 5** Thermal reconfiguration of a LC droplet comprised of a FB-E7 mixture via nematic-isotropic (N-I) phase transition. (A,D-G) Columns 1 and 2 are polarized light micrographs (single polarizer and crossed polars, respectively) of droplets of FB-E7 ( $C_{\text{FB}}=5$  % v/v) dispersed in FB-saturated aqueous 1 mM SDS solutions, upon heating across the N-I coexistence region at (A) 35.0  $^{\circ}\text{C}$ , (nematic), (D) 45.0  $^{\circ}\text{C}$ , (E) 46.0  $^{\circ}\text{C}$ , (F) 47.0  $^{\circ}\text{C}$ , and (G) 47.5  $^{\circ}\text{C}$  (isotropic), respectively. Scale bar, 10  $\mu\text{m}$ . The double-headed arrows indicate the orientation of the polarizer (P) and analyzer (A). Column 3 shows corresponding director profiles obtained from simulations, and Column 4 shows the associated (simulated) polarized light micrographs (crossed polars). The micrograph and schematic illustration in (B) and (C), respectively, show that an isotropic domain formed first at the defect at the center of the droplet upon heating.

the interfacial energy of the emulsion system. The isotropic domain was observed to adhere to the aqueous interface and shrank during cooling; with further cooling, the isotropic domain on the aqueous interface collapsed to a defect and translated back into the center to reform a single-phase nematic droplet. In comparison<sup>20</sup>, isotropic multi-compartment droplet systems reported previously do not provide control over the volume ratio of internal phases via temperature due to the immiscibility of the fluorocarbon and hydrocarbon below the upper consolute temperature and complete miscibility above this critical temperature. At temperatures below the upper consolute temperature, the volumes of the two domains of the emulsions are determined by composition.

To aid interpretation of the optical micrographs in Fig. 5 in terms of internal ordering of LC within the compartments of the Janus droplets, we performed numerical simulations of the director profiles via a Landau-de Gennes (LdG) continuum model, simulated the corresponding optical micrographs, and then compared the simulated light micrographs to our experimental observations. In particular, by matching experimental and simulated optical micrographs, we obtained information about the surface anchoring strength ( $W$ ) of the LC domains at the boundaries of the compartments of the Janus droplets. We note that the radii of the simulated droplets were 1  $\mu\text{m}$ , one order smaller than droplets observed in experiment. To enable comparisons between computation and experiments, we increased the anchoring strength by one order of magnitude to keep the ratio of anchoring energy ( $\sim Wl^2$ ) to elastic energy ( $\sim Kl$ ) unchanged. We also note that the simulation was conducted with incident light of a single wavelength, and excluded optical influences of the interface (e.g. reflection and refraction). As a result, no interference patterns (denoted by a white arrow in experimental image in Fig. 5A) were observed in simulated images.

We used an elastic modulus ( $K$ ) of 4.55 pN in the simulations. At the nematic-aqueous (N-A) interface, we specified perpendicular (homeotropic) LC anchoring consistent with our experimental observations (Fig. 5A), and  $W$  of  $1 \times 10^{-3} \text{ N m}^{-1}$ . We used these boundary conditions at all temperatures, as we observed the perpendicular orientation at the N-A interface

to be retained during heating and cooling, independent of temperature. At the N-I interface, we specified the LC to be tilted by  $50^\circ$  with respect to the surface normal (Fig. 4); we varied  $W$  at the N-I interface to obtain the best agreement between simulated and experimental optical textures. Specifically, we found that use of boundary conditions that correspond to weak anchoring ( $W = 1 \times 10^{-5} \text{ N m}^{-1}$ ) in the simulations (Columns 3 and 4 in Fig. 5) provided good agreement with experiments (Columns 1 and 2 in Fig. 5). One key observation is the absence of defects on the N-I interfaces (Fig. 5D-G) in both experiments and simulations, indicating the alignment of LC at the N-I interface can readily deviate from the easy axis (due to the elasticity of the bulk LC). If a higher anchoring strength was used in simulations to describe the N-I interface (e.g.  $W = 1 \times 10^{-4} \text{ N m}^{-1}$  and  $W = 1 \times 10^{-3} \text{ N m}^{-1}$ ), defect loops on N-I interfaces were observed, in contradiction to experiments (Fig. S8, ESI<sup>†</sup>). The absence of defects is also consistent with the minor impact of LC elasticity on the morphology of the LC compartment<sup>31</sup>, which will be addressed below. In addition, simulated optical micrographs in Fig. 5D and E show two extinction (dark) brushes between crossed polars (denoted by blue arrows), which is consistent with experiments. We also varied the orientation of the easy axis of LCs at the N-I interface from  $30^\circ$  to  $60^\circ$  to examine the sensitivity of the simulations to deviations from the experimental tilting angle ( $50^\circ$ ). We found the simulated optical texture was not sensitive to the exact tilting angle due to weak anchoring.

#### Influence of surfactant type and perfluorobenzene on internal configurations of single-phase nematic droplets

As noted in the Introduction, inspired by past studies of emulsions comprised of coexisting isotropic phases of hydrocarbons and perfluorocarbons<sup>20</sup>, a key motivation for using perfluorocarbons to induce multiple domains in LC droplets was the possibility of manipulating the morphology of the droplets via preferential adsorption of fluorocarbon and hydrocarbon surfactants at the interfaces of the domains of the droplets. As an initial step in this direction, we investigated single-phase nematic droplets to determine how SDS and perfluorooctanoic acid (PFOA) influence LC orientations at

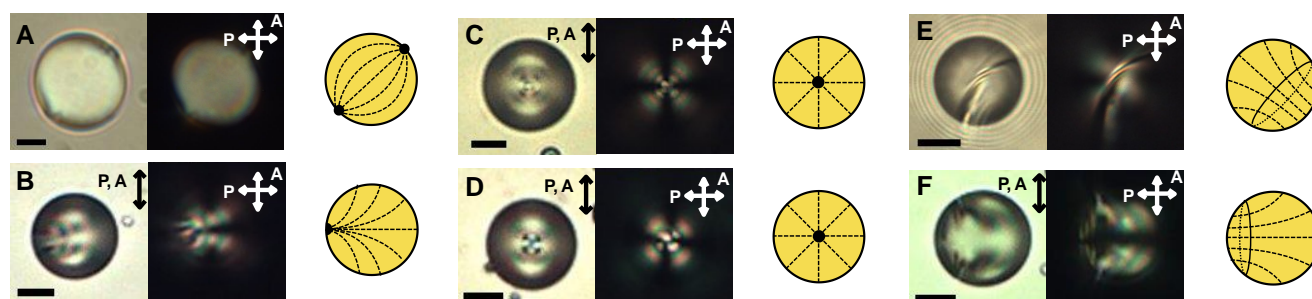


**Fig. 6** Optical micrographs showing the influence of surfactant type and concentration on the internal configurations (shown schematically to the right of the images) of nematic LC droplets (E7 or E7 + FB mixtures): (A,C,E) pure E7 and (B,D,F) FB-E7 ( $C_{\text{FB}}=5\% \text{ v/v}$ ) mixtures dispersed in aqueous solutions at  $35^\circ\text{C}$  of (A,B)  $100 \mu\text{M}$  SDS, (C,D)  $1 \text{ mM}$  SDS and (E,F)  $1 \text{ mM}$  PFOA. Scale bars,  $10 \mu\text{m}$ . The dashed black lines within the droplet boundaries in the illustrations represent the orientation of the LC director; the black dots in (A-D) represent defects; and the black solid loops in (E,F) represent line defects.

surfactant-decorated aqueous interfaces in the presence and absence of FB.

First, we address the influence of FB on anchoring in the presence of SDS surfactant. Pure E7 dispersed in aqueous 100  $\mu\text{M}$  SDS at 35  $^{\circ}\text{C}$  exhibited a “bipolar” configuration with two defects located at poles of the droplet<sup>10,34</sup> (Fig. 6A). In contrast, the FB-E7 mixture (5% v/v FB) at the same temperature, and in the presence of 100  $\mu\text{M}$  SDS, formed droplets with a director profile that radiated from a point defect located on the droplet surface (Fig. 6B). This configuration is a so-called “pre-radial” configuration<sup>10,34</sup>, consistent with a tilted alignment of LC at aqueous interface. We hypothesize that the presence of FB decreases the order of the LC at a given temperature, and thus facilitates SDS to promote the pre-radial configuration. As reported above, at higher concentrations of SDS ( $C_{\text{SDS}} = 1 \text{ mM}$  in Fig. 6C and D and also  $C_{\text{SDS}} = 2 \text{ mM}$ ), the nematic droplets comprised of E7 or FB-E7 both exhibited a radial configuration, as detailed above (Fig. 5A).

Second, in contrast to SDS, FB has only a minor impact on anchoring of E7 in the presence of PFOA surfactant at 35  $^{\circ}\text{C}$ . With aqueous 1 mM PFOA (Fig. 6E and F), the droplets in the absence and presence of FB exhibited similar configurations, as evidenced by line defects (loops in schematic illustrations in Fig. 6E and F) at a location between the equatorial plane and one of the poles of the droplets, revealing a tilted alignment of LC at aqueous interface. We note that the defect loop in the presence of FB was displaced towards the pole as compared to the LC free of FB.

The results above lead to the conclusion that, in the presence of FB, the FB-E7 mixture assumes distinct configurations in the presence of 1 mM SDS solution (Fig. 6D) and the 1 mM PFOA solution (Fig. 6F) due to differences in interfacial anchoring. We note also that the addition of PFOA caused the pH to decrease from 7 to 3, which we confirmed to not impact our experimental observations by performing control experiment at pH = 7 (Fig. S7, ESI<sup>†</sup>).

To provide boundary conditions for simulations (reported below) of the multi-phase droplets in the presence of 100  $\mu\text{M}$  SDS and 1 mM PFOA, we simulated micrometer-sized single-phase nematic droplets with increasing tilt angles at the interface. We used strong anchoring conditions ( $W = 1 \times 10^{-3} \text{ N m}^{-1}$ ) in the simulations. We define  $\theta_e$  as the tilt angle of the easy axis of the LC with respect to surface normal. For  $\theta_e = 0^{\circ}$ , the nematic droplet adopts a radial configuration with a small defect ring located in the droplet center. As  $\theta_e$  increases, the spherical symmetry breaks and the defect migrates towards the droplet surface (escaped radial configuration in Fig. 7A), until a pre-radial configuration forms for  $\theta_e$  between 45 $^{\circ}$  and 55 $^{\circ}$  (Fig. 7B). As  $\theta_e$  continues to increase, a morphological transition to an axial configuration occurs (Fig. 7C), and, finally, it evolves to a bipolar structure for  $\theta_e = 90^{\circ}$ . The dependence of defect position ( $d/R$ ) on  $\theta_e$  is shown in Fig. 7D, where  $d$  is defined as the distance between defect to droplet center. The specific tilt angles of the FB-E7 mixture in the presence of surfactants were assigned as 45 $^{\circ}$ , 60 $^{\circ}$ , 0 $^{\circ}$  and 0 $^{\circ}$  in the presence of 100  $\mu\text{M}$  SDS, 1 mM PFOA, 1 mM and 2 mM SDS, respectively, by comparing the droplet configurations obtained from experiments with

simulations (Fig. 6 and 7). We note one minor difference between our experimental observations and simulations: whereas the experiments with 1 mM PFOA led to ring defects that were displaced slightly from the equatorial plane (Fig 6E), our simulations predicted defect rings to lie on the equatorial plane (Fig. 7C). The simulations contain a number of approximations, such as the use of one elastic constant, that likely underlie this difference.

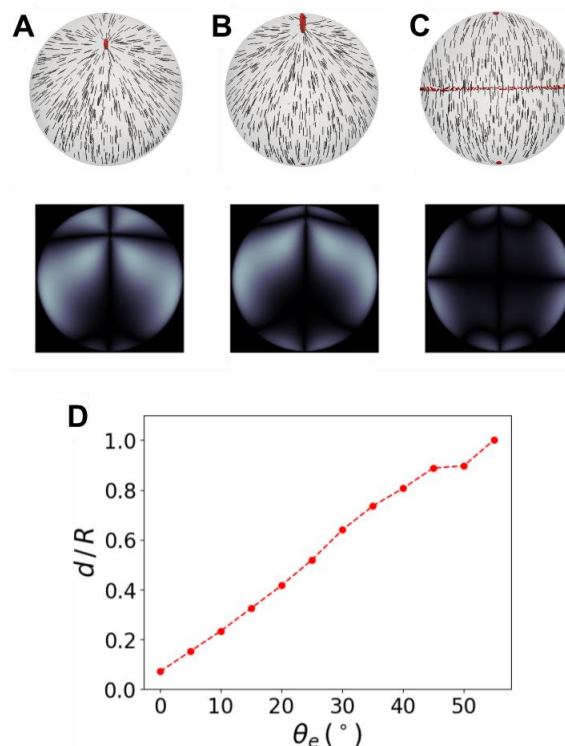


**Fig. 7** (A-C) Director fields and calculated polarized light micrographs for nematic droplets ( $R = 1 \mu\text{m}$ ,  $W = 1 \times 10^{-3} \text{ N m}^{-1}$ ) with preferred surface tilt angles of (A) 30 $^{\circ}$ , (B) 45 $^{\circ}$  and (C) 60 $^{\circ}$ , respectively. Defects are shown in red (isosurface for  $S=0.5$ ). (D) Ratio of defect-to-droplet-center distance ( $d$ ), normalized by droplet radius ( $R$ ), as a function of  $\theta_e$ .

#### Surfactant-dependent configurations of multicompartiment isotropic-LC droplets

Next, we describe results obtained using biphasic droplets. We investigated the relative influence of hydrocarbon- and fluorocarbon-based surfactants on the morphogenesis of biphasic Janus droplets, as shown in Fig. 8. We define  $\theta_I$ , the angle between N-I and I-A interfaces, as the contact angle. When using PFOA, we observed 1 mM surfactant to lead to  $\theta_I \sim 35^{\circ}$  (Fig. 8A), with a decrease in concentration of PFOA (0.5 mM) leading to an increase in  $\theta_I$  (44 $^{\circ}$ ) (Fig. S5, ESI<sup>†</sup>). This trend suggests that the interfacial tension at the I-A interface decreases more than at the N-A interface with increase in concentration of PFOA, a result that is consistent with preferential adsorption of fluorocarbon surfactant on the fluorocarbon-rich (isotropic) domain. When SDS was used (Fig. 8B-D), the effect of the surfactant was to reverse the trend:  $\theta_I$  of biphasic Janus droplets increased from 54 $^{\circ}$  to 125 $^{\circ}$  with

increase in SDS concentration. This result indicates preferential adsorption of SDS (and decrease of the interfacial tension) at the interface of the hydrocarbon-rich (nematic) domain. Overall, the opposite trend in partial wetting of the internal domains of the droplets (summarized in Fig. 8E) is consistent with an unequal distribution of FB between isotropic and nematic compartments and thus preferential adsorption of fluorocarbon and hydrocarbon surfactants on the isotropic and nematic domains, respectively. Overall, the manipulation of temperature and surface anchoring enables access to a rich range of hierarchical structures within the Janus droplets, as shown in Fig. S2-S6 of the ESI†. As discussed above, control experiments performed at both pH = 3 and pH = 7 established that the distinct droplet morphologies seen with PFOA and SDS are due to the surfactant type and not difference in pH (Fig. S7, ESI†).

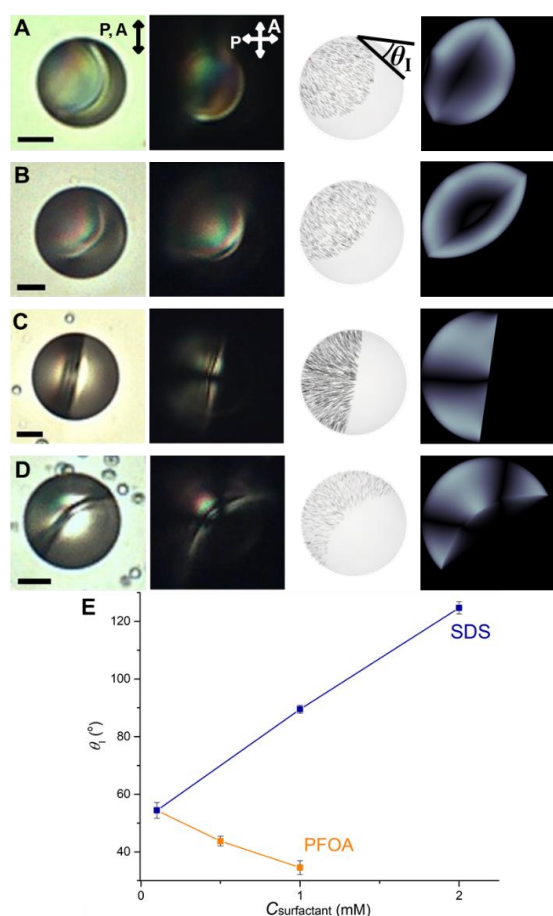


**Fig. 8** Influence of surfactant type on the morphologies of biphasic E7-FB droplets. (A-D) Columns 1 and 2 are optical micrographs (single polarizer, and crossed polars, respectively) of Janus droplets in aqueous solutions containing (A) 1 mM PFOA or (B) 100  $\mu$ M, (C) 1 mM, and (D) 2 mM SDS in N-I coexistence region. Scale bars, 10  $\mu$ m. Columns 3 and 4 show corresponding simulated director profiles and calculated polarized light micrographs. (E) Contact angles  $\theta_i$  in the presence of fluorocarbon surfactant (PFOA) versus hydrocarbon surfactant (SDS).

To understand the internal ordering of LC within the compartments, we performed numerical simulations with the LdG continuum model. We assumed that, at the N-I interface, the easy axis and the anchoring energy of LC were not affected in the presence of surfactants, that the tilt angle of the easy axis from the surface normal was  $50^\circ$  and that the anchoring energy was  $W = 1 \times 10^{-5} \text{ N m}^{-1}$  (as described above). The orientations of the LC at the aqueous interfaces were the same as those determined above from simulations, as shown in Fig. 6 and 7. We assumed these orientations to be fixed by implementing a strong anchoring strength  $W = 1 \times 10^{-3} \text{ N m}^{-1}$ . Using the simulated internal order of the droplets (Column 3 in Fig. 8A-D), we calculated the polarized light textures (Column 4 in Fig. 8A-D) and compared them to the experimental observations. We found excellent agreement (see Columns 1 and 2 in Fig. 8A-D). For example, optical textures in experiments and simulations possess no defects at N-I interfaces, and the extinction brushes and regions are consistent.

#### Additional comments on the free energies of two-phase LC-isotropic droplets

Our observation that the biphasic Janus droplets with nematic and isotropic compartments assume spherical shapes suggests that  $\gamma_{13} \sim \gamma_{23} \gg \gamma_{12}$  (Fig. 1). To test this interpretation, we separated coexisting nematic and isotropic phases of a FB-E7 (8% v/v FB) mixture at 36  $^\circ\text{C}$  by centrifugation. We used the 8% v/v mixture to ensure that the N-I temperature interval was in the operational temperature range of the centrifuge ( $-10^\circ\text{C}$  to  $40^\circ\text{C}$ ). The density of the nematic phase ( $1.0462 \text{ g cm}^{-3}$ ) was slightly lower than that of the isotropic phase ( $1.0487 \text{ g cm}^{-3}$ ) at  $36^\circ\text{C}$ . Next we measured the interfacial tensions of the nematic-aqueous interface,  $\gamma_{\text{NA}}$ , the isotropic-aqueous interface,  $\gamma_{\text{IA}}$ , and the nematic-isotropic interface,  $\gamma_{\text{NI}}$ , using the pendant drop method. The results, shown in Fig. 9, indicate that the orders of magnitude of  $\gamma_{\text{NA}}$  and  $\gamma_{\text{IA}}$  are  $1 \text{ mN m}^{-1}$ , and the two interfacial tensions were numerically indistinguishable. In contrast, the magnitude of  $\gamma_{\text{NI}}$  was  $10^{-2} \text{ mN m}^{-1}$  ( $4 \pm 2 \times 10^{-2} \text{ mN m}^{-1}$ ), which is two orders of magnitude smaller than  $\gamma_{\text{NA}}$  and  $\gamma_{\text{IA}}$ . The magnitude of  $\gamma_{\text{NI}}$  is in good agreement with that of other thermotropic LCs reported elsewhere<sup>59</sup>. Although the interfacial tensions of the N-I interfaces were low, the density difference between the two phases was also low, thus giving rise to accurate determination of interfacial tension based on analysis of droplet shape. Overall, the three interfacial tensions satisfy the thermodynamic criteria,  $\gamma_{\text{NA}} \sim \gamma_{\text{IA}} \gg \gamma_{\text{NI}}$ , for spherical Janus droplets. Although the negative slopes of the plots shown in Fig. 9 for both SDS and PFOA indicate a positive surface excess concentration of these surfactants at the aqueous interfaces, a quantitative interpretation is challenging for a number of reasons. For example, we note that PFOA may not completely dissociate at pH = 3, and that addition of surfactants may lead to redistribution of FB molecules in this FB-E7 multi-component system.

For droplets with size ( $l$ ) of 10  $\mu\text{m}$ , we use the results described above to calculate that the overall free energy of the N-I interface ( $\sim \gamma l^2$ ) is  $\sim 10^{-15} \text{ J}$ , and the anchoring energy (orientation-dependent

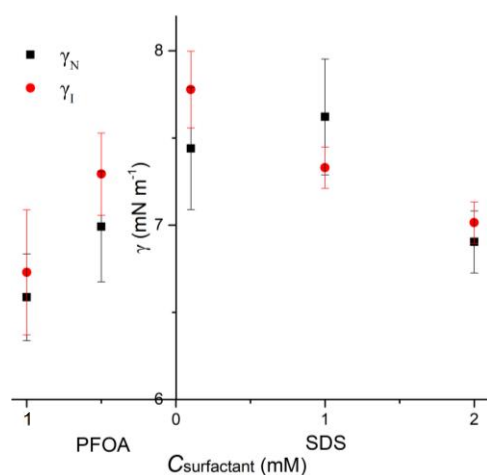


**Fig. 9** Interfacial tensions between nematic-aqueous and isotropic-aqueous interfaces,  $\gamma_{NA}$  and  $\gamma_{IA}$ , respectively using the pendant drop method. Mean  $\pm$  s.d. ( $n = 3$ ) are shown.  $\gamma_{NA}$  and  $\gamma_{IA}$  are significantly larger than N-I interfacial tension,  $\gamma_{N-I}$  ( $4 \pm 2 \times 10^{-2}$  mN m<sup>-1</sup>).

contribution) is  $\sim 10^{-17}$  J; at the nematic-aqueous interface, the overall interfacial free energy ( $\sim \gamma l^2$ ) is  $\sim 10^{-13}$  J, and the anchoring energy is  $\sim 10^{-15}$  J. When compared to the elastic energy ( $\sim Kl$ ), which is  $\sim 10^{-17}$  J, the interfacial free energies dominate the shapes of nematic domains in the coexistence region for E7-FB mixtures, as evidenced by the spherical (Fig. 4C) and cylindrical (Fig. 4D) shape of the nematic domains. The dominating interfacial energies are also responsible for the spherical morphologies of the droplets comprising coexisting N-I phases dispersed in water (Fig. 5 and 8). In addition, for the pendant drop measurements reported above (using droplets with  $l \sim 1$  mm), the elastic energy ( $Kl \sim 10^{-15}$  J) is unlikely to significantly influence the determination of interfacial tension ( $\gamma l^2 \sim 10^{-9}$ - $10^{-11}$  J).

## Conclusions

We report that mixtures of FB-E7 dispersed in an aqueous continuous phase form emulsion droplets that exhibit stable Janus morphologies comprised of coexisting nematic and isotropic oil domains. Partial miscibility of FB and E7 leads to a broad temperature range over which the nematic (N) and isotropic (I) phases coexist within the droplets, enabling facile and reversible control of the volumes of each compartment of the Janus droplets. We note that this characteristic of the system is challenging to realize in isotropic emulsion systems<sup>20</sup>. Significantly, the similarity in composition of the N and I domains within the droplets leads to N-I interfacial tensions that are lower than the aqueous interfacial tensions in the system, which results in droplets that maintain their spherical shape during changes in internal morphology induced by variations in temperature or interfacial adsorbates (surfactants). For the latter case, the droplet morphology was tuned by using hydrocarbon and fluorocarbon surfactants. As compared to isotropic multiphase droplets, the presence of the LC domain was shown to lead to morphology-dependent optical

signatures. These optical signatures were largely reproduced by simulations based on a Landau-de Gennes free energy. Additional studies are needed, however, to understand why the additional of FB leads to changes in interfacial anchoring of the LC phases at aqueous interfaces. Although the majority of results presented in this paper were obtained using the nematic LC called E7, qualitatively similar results have been obtained with other nematic LCs, including nematic phases of 5CB, 8CB and TL205. We anticipate that the approach demonstrated in this paper can be extended in future studies to LC phases other than achiral nematics, including cholesteric, smectic and blue phases. Ongoing experiments are also exploring the dynamics of the transitions between morphological states that are triggered by changes in surfactant concentration and type. We comment that the influence of surfactant architecture (e.g., use of bolaform surfactants) on the orientational anchoring of LCs may also yield morphologies of droplets that go beyond those reported here<sup>60</sup>. Overall, the results reported in this paper advance the design of reconfigurable soft matter systems based on isotropic perfluorocarbon oils and nematic LCs.

## Conflicts of interest

There are no conflicts to declare.

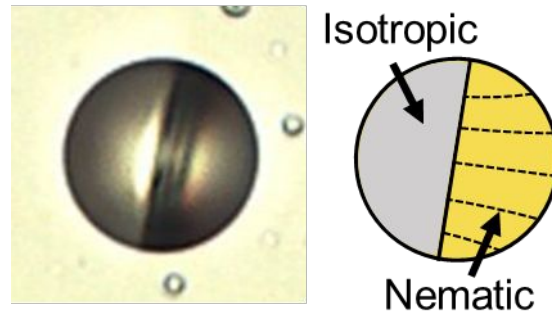
## Acknowledgements

The authors acknowledge support from the Department of Energy, Basic Energy Sciences, Division of Materials Research, Biomaterials Program under Grant No. DE-SC0004025. YY acknowledges partial fellowship support from the Department of Chemical and Biological Engineering at University of Wisconsin-Madison.

## Notes and references

- 1 K. J. Lissant, *Emulsions and emulsion technology*, Marcel Dekker, New York, vol. 6., 1974.
- 2 M. A. Augustin and Y. Hemar, *Chem. Soc. Rev.*, 2009, **38**, 902–912.
- 3 P. A. Gresham, M. Barnett, S. V. Smith and R. Schneider, *Nature*, 1971, **234**, 149–150.
- 4 E. Bukusoglu, M. Bedolla Pantoja, P. C. Mushenheim, X. Wang and N. L. Abbott, *Annu. Rev. Chem. Biomol. Eng.*, 2016, **7**, 163–196.
- 5 X. Wang, E. Bukusoglu, D. S. Miller, M. A. Bedolla Pantoja, J. Xiang, O. D. Lavrentovich and N. L. Abbott, *Adv. Funct. Mater.*, 2016, **26**, 7343–7351.
- 6 A. S. Utada, E. L. Lorraineau, D. R. Link, P. D. Kaplan, H. A. Stone and D. A. Weitz, *Science*, 2005, **308**, 537–541.
- 7 N. Pannacci, H. Bruus, D. Bartolo, I. Etchart, T. Lockhart, Y. Hennequin, H. Willaime and P. Tabeling, *Phys. Rev. Lett.*, 2008, **101**, 1–4.
- 8 J. A. Hanson, C. B. Chang, S. M. Graves, Z. Li, T. G. Mason and T. J. Deming, *Nature*, 2008, **455**, 85–88.
- 9 P. S. Drzaic, *Liquid crystal dispersions. Vol.1*, World Scientific, 1995.

- 10 J. K. Gupta, J. S. Zimmerman, J. J. De Pablo, F. Caruso and N. L. Abbott, *Langmuir*, 2009, **25**, 9016–9024.
- 11 J. A. Moreno-Razo, E. J. Sambriski, N. L. Abbott, J. P. Hernández-Ortiz and J. J. De Pablo, *Nature*, 2012, **485**, 86–89.
- 12 E. Bukusoglu, X. Wang, Y. Zhou, J. A. Martínez-González, M. Rahimi, Q. Wang, J. J. de Pablo and N. L. Abbott, *Soft Matter*, 2016, **12**, 8781–8789.
- 13 I.-H. Lin, D. S. Miller, P. J. Bertics, C. J. Murphy, J. J. de Pablo and N. L. Abbott, *Science*, 2011, **332**, 1297–1300.
- 14 Y. Kim, X. Wang, P. Mondkar, E. Bukusoglu and N. L. Abbott, *Nature*, 2018, **557**, 539.
- 15 T. Bera and J. Fang, *Langmuir*, 2013, **29**, 387–392.
- 16 L. E. Aguirre, A. de Oliveira, D. Seč, S. Čopar, P. L. Almeida, M. Ravnik, M. H. Godinho and S. Žumer, *Proc. Natl. Acad. Sci.*, 2016, **113**, 1174–1179.
- 17 S. Torza and S. G. Mason, *Science*, 1969, **163**, 813–814.
- 18 J. Guzowski, P. M. Korczyk, S. Jakiela and P. Garstecki, *Soft Matter*, 2012, **8**, 7269.
- 19 T. Nisisako and T. Hatsuzawa, *Microfluid. Nanofluidics*, 2010, **9**, 427–437.
- 20 L. D. Zarzar, V. Sresht, E. M. Sletten, J. A. Kalow, D. Blankschtein and T. M. Swager, *Nature*, 2015, **518**, 520–524.
- 21 X. Wang, Y. Zhou, Y.-K. Kim, D. S. Miller, R. Zhang, J. A. Martínez-González, E. Bukusoglu, B. Zhang, T. M. Brown, J. J. de Pablo and N. L. Abbott, *Soft Matter*, 2017, **13**, 5714–5723.
- 22 F. Mondiot, X. Wang, J. J. de Pablo and N. L. Abbott, *J. Am. Chem. Soc.*, 2013, **135**, 9972–9975.
- 23 M. A. Gharbi, M. Nobili and C. Blanc, *J. Colloid Interface Sci.*, 2014, **417**, 250–255.
- 24 X. Wang, D. S. Miller, J. J. de Pablo and N. L. Abbott, *Soft Matter*, 2014, **10**, 8821–8828.
- 25 X. Wang, D. S. Miller, J. J. De Pablo and N. L. Abbott, *Adv. Funct. Mater.*, 2014, **24**, 6219–6226.
- 26 J. K. Whitmer, X. Wang, F. Mondiot, D. S. Miller, N. L. Abbott and J. J. De Pablo, *Phys. Rev. Lett.*, 2013, **111**, 1–5.
- 27 M. Urbanski, C. G. Reyes, J. Noh, A. Sharma, Y. Geng, V. Subba Rao Jampani and J. P. F. Lagerwall, *J. Phys. Condens. Matter*, 2017, **29**, 133003.
- 28 E. Bukusoglu, X. Wang, J. A. Martínez-González, J. J. De Pablo and N. L. Abbott, *Adv. Mater.*, 2015, **27**, 6892–6898.
- 29 A. Fernández-Nieves, D. R. Link, M. Márquez and D. A. Weitz, *Phys. Rev. Lett.*, 2007, **98**, 1–4.
- 30 D. Seč, T. Porenta, M. Ravnik and S. Žumer, *Soft Matter*, 2012, **8**, 11982.
- 31 Y. K. Kim, S. V. Shiyankovskii and O. D. Lavrentovich, *J. Phys. Condens. Matter*, 2013, **25**, 404202.
- 32 Y.-K. Kim, B. Senyuk, S.-T. Shin, A. Kohlmeier, G. H. Mehl and O. D. Lavrentovich, *Soft Matter*, 2014, **10**, 500–509.
- 33 Y. Zhou, E. Bukusoglu, J. A. Martínez-González, M. Rahimi, T. F. Roberts, R. Zhang, X. Wang, N. L. Abbott and J. J. De Pablo, *ACS Nano*, 2016, **10**, 6484–6490.
- 34 G. E. Volovik and O. D. Lavrentovich, *Zh Eksp Teor Fiz*, 1983, **85**, 1997–2010.
- 35 P. Poulin and D. A. Weitz, *Phys. Rev. E*, 1998, **57**, 626–637.
- 36 T. Lopez-Leon and A. Fernandez-Nieves, *Phys. Rev. E*, 2009, **79**, 1–5.
- 37 T. Lopez-Leon, V. Koning, K. B. S. Devaiah, V. Vitelli and A. Fernandez-Nieves, *Nat. Phys.*, 2011, **7**, 391–394.
- 38 D. Seč, T. Lopez-Leon, M. Nobili, C. Blanc, A. Fernandez-Nieves, M. Ravnik and S. Žumer, *Phys. Rev. E*, 2012, **86**, 1–4.
- 39 H. Liang, J. Noh, R. Zentel, P. Rudquist, P. F. Jan and J. P. Lagerwall, *Philos. Trans. R. Soc. A Math. Phys. Eng. Sci.*, 2013, **371**, 20120258.
- 40 T. Lopez-Leon, A. Fernandez-Nieves, M. Nobili and C. Blanc, *J. Phys. Condens. Matter*, 2012, **24**, 284122.
- 41 A. Darmon, M. Benzaquen, D. Seč, S. Čopar, O. Dauchot and T. Lopez-Leon, *Proc. Natl. Acad. Sci.*, 2016, **113**, 9469–9474.
- 42 J. Jeong, A. Gross, W.-S. Wei, F. Tu, D. Lee, P. J. Collings and A. G. Yodh, *Soft Matter*, 2015, **11**, 6747–6754.
- 43 G. A. Oweimreen and M. Hasan, *Mol. Cryst. Liq. Cryst.*, 1983, **100**, 357–371.
- 44 I. M. Tang and S. Denprayoonwong, *Phys. Lett. A*, 1988, **127**, 435–437.
- 45 M. A. Gidley and D. Stubley, *J. Chem. Thermodyn.*, 1982, **14**, 785–790.
- 46 M. A. Gidley and D. Stubley, *J. Chem. Thermodynamics*, 1986, **18**, 595–600.
- 47 P. G. de Gennes and J. Prost, *The Physics of Liquid Crystals*, Clarendon Press, 1993.
- 48 M. Kleman and O. D. Lavrentovich, *Soft Matter Physics: An Introduction*, Springer, New York, NY, USA, 2003.
- 49 J. B. Fournier and P. Galatola, *Europhys. Lett.*, 2005, **72**, 403–409.
- 50 M. Ravnik and S. Žumer, *Liq. Cryst.*, 2009, **36**, 1201–1214.
- 51 R. Ondris-Crawford, E. P. Boyko, B. G. Wagner, J. H. Erdmann, S. Žumer and J. W. Doane, *J. Appl. Phys.*, 1991, **69**, 6380–6386.
- 52 D. S. Seo, K. I. Muroi, T. R. Isogami, H. Matsuda and S. Kobayashi, *Jpn. J. Appl. Phys.*, 1992, **31**, 2165–2169.
- 53 S. D. Kim, B. Lee, S. W. Kang and J. K. Song, *Nat. Commun.*, 2015, **6**, 1–8.
- 54 K. Shimizu, M. F. C. Gomes, A. A. H. Padua, L. P. N. Rebelo and J. N. C. Lopes, *J. Phys. Chem. B*, 2009, **113**, 9894–9900.
- 55 C. R. Patrick and G. S. Prosser, *Nature*, 1960, **187**, 1021.
- 56 Y.-K. Kim, G. Cukrov, J. Xiang, S.-T. Shin and O. D. Lavrentovich, *Soft Matter*, 2015, **11**, 3963–3970.
- 57 J. M. Brake and N. L. Abbott, *Langmuir*, 2002, **18**, 6101–6109.
- 58 X. Wang, D. S. Miller, E. Bukusoglu, J. J. De Pablo and N. L. Abbott, *Nat. Mater.*, 2016, **15**, 106–112.
- 59 S. Faetti and V. Palleschi, *Phys. Rev. A*, 1984, **30**, 3241–3251.
- 60 F. P. Hubbard and N. L. Abbott, *Langmuir*, 2007, **23**, 4819–4829.



For Table of Contents Only

We report formation of Janus droplets with coexisting liquid crystalline and isotropic compartments, stable spherical shapes, and widely tunable internal morphologies.